



Template-based sputtering method for vertically aligned Tin nanotube arrays: From fabrication to superconductivity

Changli Li ^a, Maojun Zheng ^{a,*}, Ming Li ^a, Changqing Zhu ^a, Li Ma ^b, Xianghu Wang ^c, Zhengping Li ^a, Wenzhong Shen ^a

^a Laboratory of Condensed Matter Spectroscopy and Opto-Electronic Physics, Department of Physics, Shanghai Jiao Tong University, Shanghai, 200240, People's Republic of China

^b School of Chemistry & Chemical Technology, Shanghai Jiao Tong University, Shanghai, 200240, People's Republic of China

^c School of Mechanical Engineering, Shanghai Dianji University, Shanghai, 200240, People's Republic of China

ARTICLE INFO

Article history:

Received 20 November 2012

Received in revised form 28 May 2013

Accepted 29 May 2013

Available online 14 June 2013

Keywords:

AAO

Magnetron sputtering

Substrate temperature

Self-Assembly

Sn nanotube array films

Superconductivity

ABSTRACT

Large-scale Tin (Sn) nanotube arrays have been fabricated using template-based sputtering method. By controlling the growth temperature, two kinds of Sn films with either cross-linked or isolated nanotube arrays can be prepared after removal of anodic alumina oxide film. Morphology-dependent superconducting properties and pinning effect of magnetic flux were observed. The magnetic property of the isolated Sn nanotube arrays is similar to the single-crystal Sn nanowires while cross-linked Sn nanotube arrays exhibit a typical magnetic property of hard superconductor. This method could provide a low-cost and convenient approach to the fabrication of large-scale ordered metal nanostructures with desirable function.

© 2013 Elsevier B.V. All rights reserved.

1. Introduction

One-dimensional (1D) semiconductor nanostructures such as nanotubes, nanorods, nanowires and nanobelts have attracted considerable attention due to their unique physical and chemical properties for the possible use in field-effect transistor [1,2], optoelectronic sensors [3,4], solar cells [5,6], photoelectrochemical cells [7,8] and piezotronics [9]. Meanwhile, metallic nanostructures have also been considered as one of the most promising materials for extensive applications, including electrocatalysis [10,11], molecular detection [12] and nanobiosensing [13]. Therefore, Engineering the shape, size and assembly of 1D metallic nanostructured materials is an important aspect of nanofabrication, which describes the coupling between the design and application of nanodevices.

Up to now, studies of superconducting properties of metallic Tin nanowires have revealed very interesting behavior associated with their reduced physical dimension [14–16]. The onset critical field (H_c) and transition temperature (T_c) can be significantly affected by the diameter and crystal textures of the nanowires. In addition, the superconductivity of other Sn nanostructures such as nanosquares and nanodisks have also been investigated and shape-dependent

superconducting properties were observed [17]. However, the study of the preparation and superconductivity of Sn nanotubes is seldom involved.

Porous-template such as anodic alumina oxide (AAO) membrane has been extensively used as an easy way to fabricate ordered nanowire and nanotube arrays that possess various length, diameter and gap by choosing appropriate anodization conditions [18,19]. However, AAO membranes without the support of barrier layer and Al substrate are fragile and thus difficulty of handling. More importantly, dissolving of the membrane usually lead to the collapse of the nanostructures because of attractive forces between the nanowire/nanotubes and big bundles are formed due to the sticking together of the nanostructures. Thus, the potential applications of these nanostructures in the field of optical sensors and nanobiological devices may be delayed by the changing of period and orientation. Here we report the use of AAO film (with Al substrate) as a template for fabricating ordered arrays of Sn nanotubes. It is found that the film's properties can be tuned by adjusting the template temperature during sputtering. Thus, two different free-standing and transferable Sn films with ordered nanotube arrays were fabricated by controlling the substrate temperature. Fig. 1(a) and (b) show the schematic diagram of the two kinds of nanotube arrays formed at room temperature (RT) and 250 °C without the support of AAO template, respectively. The superconducting properties of these nanotube arrays were also measured. In our experiments, morphology-dependent superconducting properties and pinning effect are observed. The results suggest that this method maybe a low-cost

* Corresponding author. Tel.: +86 021 34202791.

E-mail address: mjzheng@sjtu.edu.cn (M. Zheng).

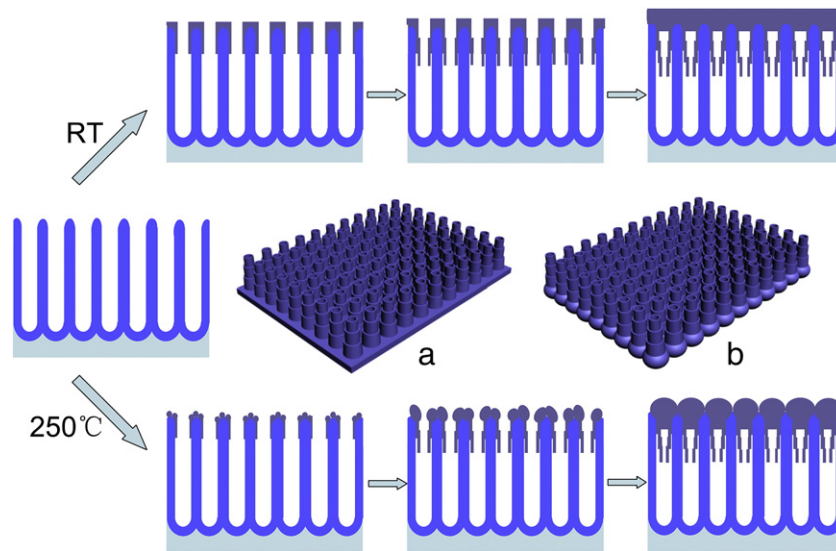


Fig. 1. Preparation progress of Sn films with vertically aligned nanotube arrays obtained at RT and 250 °C, respectively. (a)–(b) Schematic diagram of the cross-linked and isolated Sn nanotube arrays formed at RT and 250 °C after removing AAO film, respectively.

and convenient way to prepare a large variety of self-assembly metal nanostructures showing desirable performance.

2. Experimental section

2.1. Fabrication of AAO template

The AAO templates were prepared through stable anodization of high purity Al foil (99.999%) by the two-step process [20–22]. Before anodization, aluminum foil was ultrasonically cleaned in acetone for 15 min and washed in deionized water and then electropolished at a constant voltage (10V) for 5 min in a solution of HClO_4 and $\text{C}_2\text{H}_5\text{OH}$ ($v/v = 1:4$) at room temperature. The prepared Al foil was first anodized in $\text{H}_3\text{PO}_4\text{-C}_2\text{H}_5\text{OH-H}_2\text{O}$ electrolyte system (0.25 M H_3PO_4 , -5°C , 195V) for 2 min. The resulting nanoporous film on the foil was then removed by chromic acid (H_2CrO_4), leaving hexagon-like footprints on the surface of the foil. A second anodization was then performed under the same condition for 2 min to prepare ordered AAO nanopore film with a large pore diameter of ~ 170 nm and interpore spacing of ~ 350 nm.

2.2. Deposition of Sn films

Sn films were deposited on AAO substrates by DC magnetron sputtering using a circular tin target (diameter: 60 mm; purity: 99.99%). In detail, the working chamber was pumped lower than 2×10^{-3} Pa before sputtering, the substrate holder was at a distance of 6 cm from the target and the applied sputtering power is maintained at 24 W. The argon flow was adjusted to 10 sccm and kept the gas pressure of 0.85 Pa during sputtering. The sputtering time was fixed at 1 min, 2 min, 3 min and 4 min at RT and 30 s, 1 min, 2 min and 3 min at 250 °C, respectively.

2.3. Characterization

The morphologies of the films were investigated by using field-emission scanning electron microscope with a operating voltage of 5 kV (FE-SEM, Philips Sirion 200, Philips, Holland, Netherlands). The structural properties were determined using a D8 DISCOVER X-ray diffractometer (XRD) with Cu $K\alpha$ radiation (voltage: 40 kV, current: 40 mA). The out-of-plane orientation was determined in the Bragg-Brentano configuration. The superconducting properties were measured by

physical property measurement system (PPMS) - 9T(II). The magnetic field for moment versus time (M–T) curve is 0.01 T and the temperature for moment versus magnetic field (M–H) is 2 K.

3. Results and discussion

Tin was deposited by using magnetron sputtering on an AAO template. The morphologies of the AAO template were characterized by FE-SEM. Fig. 2(a) and (b) show the top-view and cross-section view images of an AAO template, respectively. Hexagonally nanopore arrays with an average diameter of 170 nm and interpore distance of 350 nm are obtained. It is clear that every nanopore has a conical opening and all parallel channels at a uniform diameter (as shown in Fig. 2(b)). Fig. 2(c–f) show SEM images of Sn deposited on AAO templates with substrate temperature of 250 °C, sputtering power of 24 W and varying sputtering time t . For $t = 0.5, 1$ and 2 min, the nanoporous structure of the AAO film is clearly visible. For $t = 0.5$ min, the deposited Sn film is composed of isolated nanoaggregates with an average size of ca. 75 nm (Fig. 2c). Smaller nanoaggregates are observed on the sidewall of nanochannel (inset of Fig. 2c). For longer sputtering time ($t = 1$ and 2 min), larger nanoaggregates are observed and their mean size increases to 115 nm and 175 nm when t is increased from 1 min to 2 min, respectively (Fig. 2d and e). The inset of Fig. 2d and e (cross-section view) clearly present that those Sn nanoaggregates hang slightly over the pore edges. At the longest t (3 min, Fig. 2f), the nanoporous structure of the AAO film is no longer observed and an ordered array which constitute of isolated Sn nanocrystal (ca. 250 nm) is obtained. These Sn nanocrystals feed the opening of the nanopore to the full and isolated from one another, which could be confirmed by its large sheet resistance (> 15 M Ω). This metal film can be transformed onto different substrate through the connecting of conducting silver glue and then detached from the AAO film by dissolving the Al substrate and alumina membrane. Fig. 3 shows the top-view and cross-section FE-SEM images of Sn film with vertically aligned and isolated nanotube arrays which detached from the AAO film and then transformed on tin-doped indium oxide (ITO)/glass substrate. Fig. 3a is the tilted view of the Sn nanotube arrays, it is note that the period of the nanotube arrays is 350 nm, which is consistent with the period of the AAO film. The image with higher magnification is shown in Fig. 3b and nanotube structure can be observed clearly. Fig. 3c shows the top-view of the Sn nanotube arrays, from which the nanotube possessing a gradient-changing diameter of length about 500 nm and

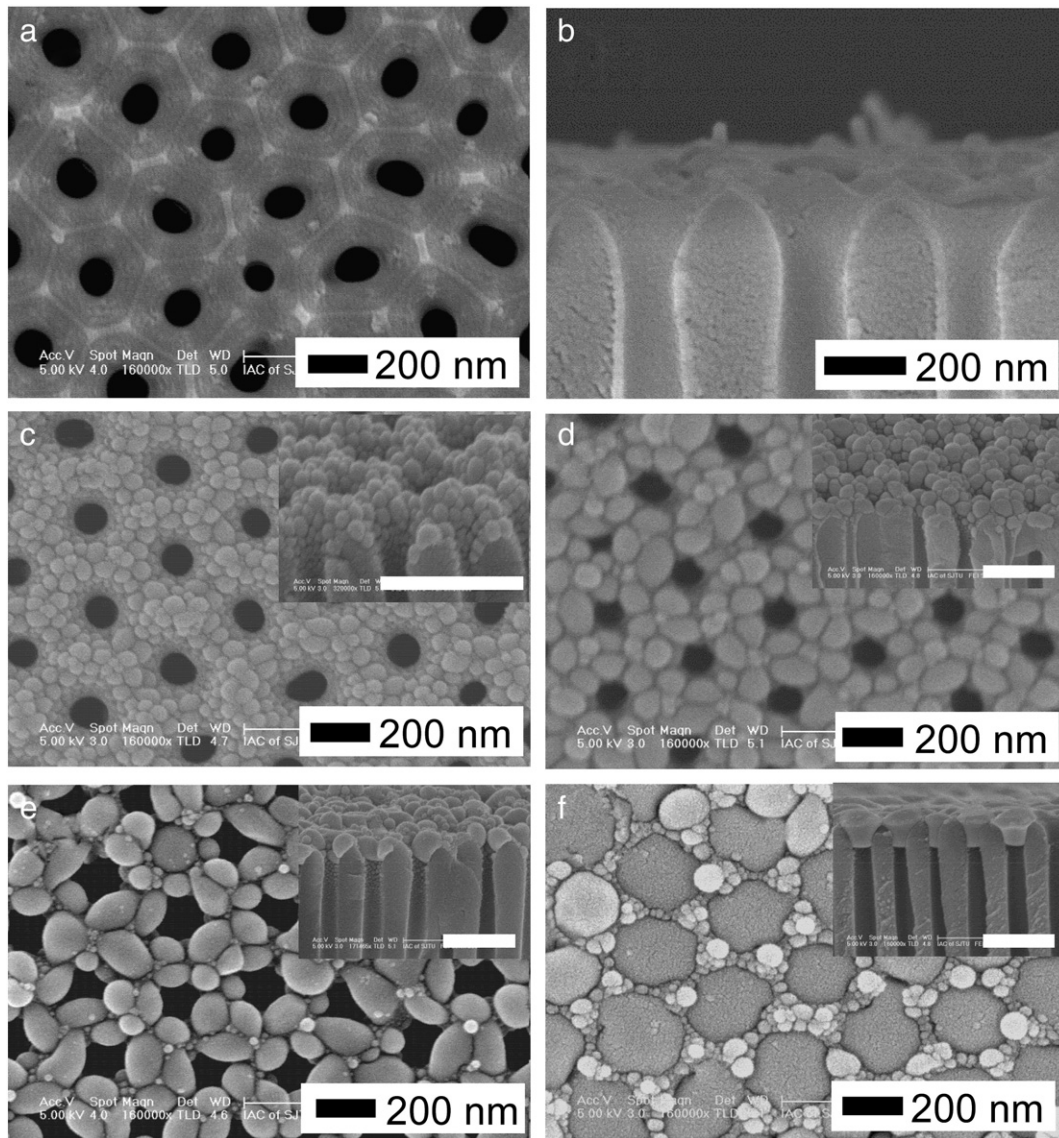


Fig. 2. SEM images of AAO template and Sn deposited on AAO template at 250 °C. (a)–(b) top view and cross-section of the AAO template. (c)–(f) Sn deposited onto AAO template with a time of 30 s, 1 min, 2 min, 3 min, respectively. The top-right insets are the cross-section view (scale bar = 500 nm).

thickness of about 15 nm was found. The white arrows pointed in Fig. 3c indicate that the whole nanotube is composed of three segments corresponding to diameter of 80, 100 and 175 nm (from top to bottom). The cross-section view presents that the bottom of the nanotube is a solid nanocrystal, as shown in Fig. 3d, which also could be found in the inset of Fig. 2f. The nanotube nanostructure could not be observed in the inset of Fig. 2f because of the detachment of nanotube induced by the mechanical shear of AAO template during cross-section specimen preparation process.

Fig. 4 show FE-SEM images of Sn films obtained at RT and different t , ranging from 1 to 4 min with an increment of 1 min. It is observed that the film morphology changes gradually with t . For $t = 1$ min (Fig. 4a), the obtained Sn films reproduce the substrate geometry of AAO template and the pore diameter (~ 130 nm) of Sn nanopore film is smaller than the pore size (~ 170 nm) of the AAO substrate. Increasing t to 2 min (Fig. 4b) and 3 min (Fig. 4c) the pore diameter of obtained films become smaller and some pores are blocked. For $t = 4$ min, the characteristic morphology of the underlying AAO film is not observed and continuous Sn film without pore structure is formed, as shown in Fig. 4d. The cross-section of the Sn films prepared at different time

can be found in the inset of Fig. 4(a)–(d), respectively. Fig. 5 show the FE-SEM images of this continuous Sn film after the removal of AAO template. Fig. 5a and b are the low magnification and high magnification images (tilted view) of the vertically aligned Sn nanotube arrays, respectively. The length of the nanotubes is about 500 nm. The top-view image (Fig. 5c) also shows the nanotubes possess a changing diameter along the growth direction which is in consistent with the specimen fabricated at the temperature of 250 °C. The cross-section image shows that the nanotubes are cross-linked, as shown in Fig. 5d. The fraction section (the inset of Fig. 5d) of the nanotube arrays indicates that the nanotubes have a homogeneous hollow structure.

The growth process could be explained by the effect of substrate temperature on the surface energy. If the substrate temperature is high enough metals could spontaneously self-assemble at the surface of the substrate to minimize the overall energy of the system [23,24]. For low-melting-point metal like Sn, room temperature is enough to promote coalescence during low-energy deposition such as thermal evaporation [25]. However, by means of magnetron sputtering, the deposited Sn film exhibits wetting property (i.e., the film reproduces the substrate geometry) at RT deposition, higher temperature is necessary

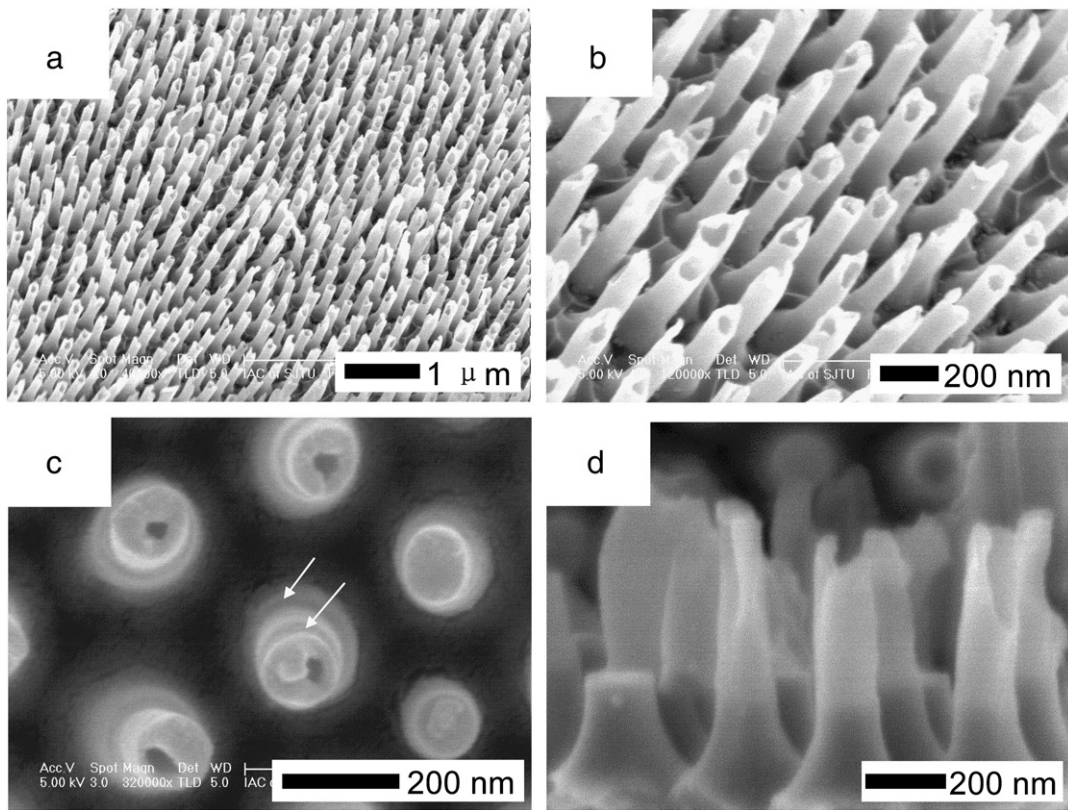


Fig. 3. SEM images of isolated Sn nanotube arrays formed at 250 °C and detached from AAO template: (a)–(b) low magnification and large magnification tilted view of the nanotube arrays, respectively, (c) top view, (d) cross-section view.

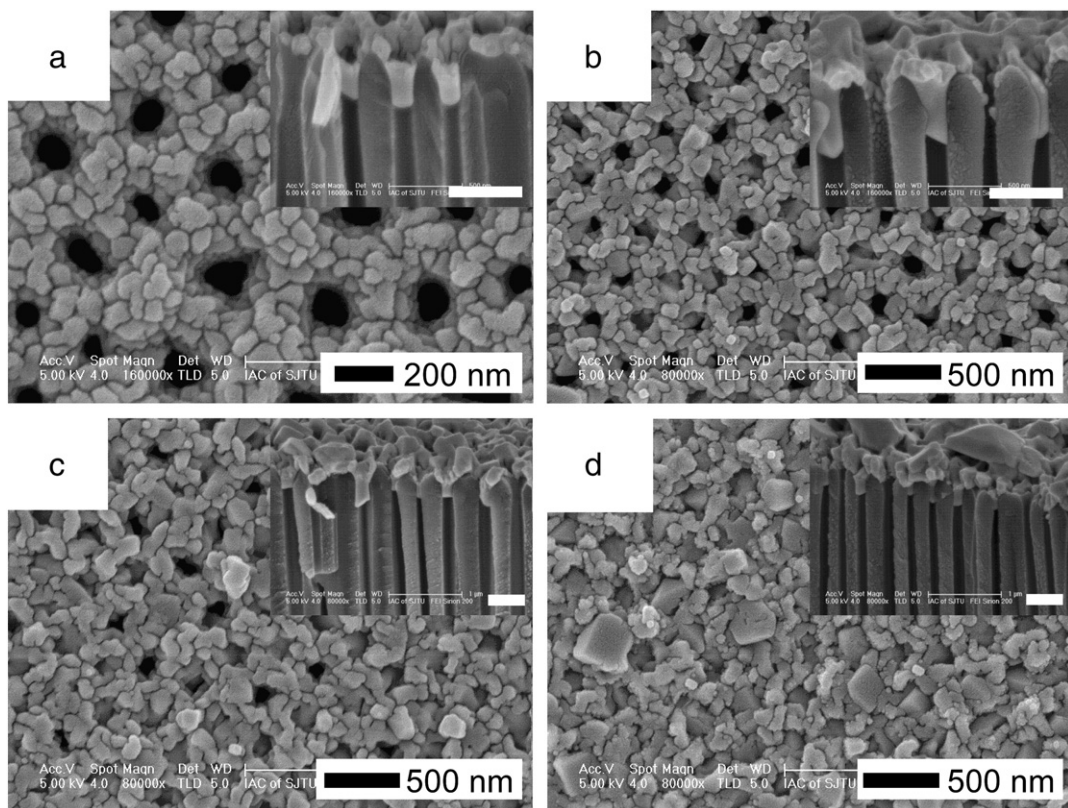


Fig. 4. SEM images of Sn deposited on AAO template at RT. (a)–(d) Sn deposited onto AAO template with a time of 1 min, 2 min, 3 min, 4 min, respectively. The top-right insets are the cross-section view (scale bar = 500 nm).

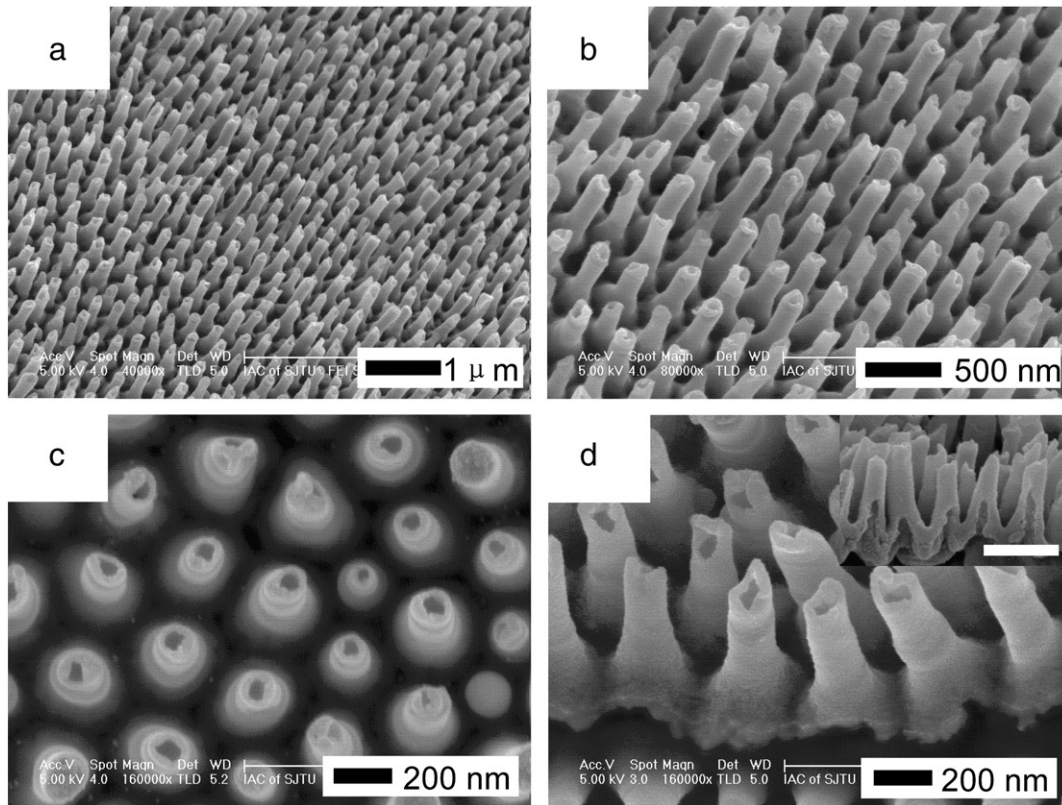


Fig. 5. SEM images of cross-linked Sn nanotube arrays formed at RT and detached from AAO template: (a)–(b) low magnification and large magnification tilted view of the nanotube arrays, respectively, (c) top view, (d) cross-section view. The inset is the fracture section of the nanotube arrays (scale bar = 500 nm).

for the spontaneously self-reorganization of the deposited Sn. The proposed mechanism of growth of the nanotube is shown in Fig. 1. When the substrate temperature is maintained at RT, due to the stronger attractive force between anion impurities and Sn ions compared to thermal evaporation, the metal ions will deposit onto the top surface of the AAO template and nanocrystal arrays cannot be formed. Meanwhile, Sn ions will deposit into the nanopores and stick onto the sidewall of the nanopores, then the first Sn layer is formed. The subsequent layer is formed by the Sn ions continue to deposit onto the former layer and extend along the growth direction. As the deposition progressing, the pore of Sn film finally closes meanwhile the growth of nanotube terminates. With a substrate temperature of 250 °C, the growth process of Sn nanotube in the nanopore of AAO is consistent with the specimen prepared at RT while the Sn ions deposit on the top surface of AAO exhibit a completely different growth mechanism. With ion motion being favored at the surface of substrate by higher temperature, the surface reorganization and minimization of the energy of the whole system were achieved. Thus, small Sn nanocrystals formed on the necks between nanopores at the beginning of the deposition, and then the nanocrystals become bigger and decrease in number as the time goes on. Eventually, individual nanocrystals bigger than the pore diameters form an ordered array over the nanopores of AAO.

The mechanism of the growth of size-changing nanotube inside the AAO nanopores is not so clear at this stage. But a growth mechanism related to capillary condensation occurred in AAO nanopores during the deposition can probably be proposed to describe this phenomenon. In recent years, the filling behavior of vapor and solvent in the nanopores has been studied by using AAO films as a porous medium [26–28]. The system presented a pronounced hysteretic capillary filling of the gas/liquid in the nanopores and eventually a partially filled pore with meniscus was formed. In the case of film deposition on AAO template, Losic et al. [29] found that the gold nanorods with a conical

structure embedded in AAO nanopores were formed during the thermal evaporation and the formation mechanism can probably be attributed to the capillary condensation theory. In our experiment, we infer a similar multilayer hysteretic capillary filling was occurred in the AAO nanopores (as shown in Fig. 1). However, the magnetron sputtering is a fast deposition process so that the growth of the diameter-changing structures terminates early as the top opening of AAO template closes. Thus, a diameter-changing nanotube structures instead of the conical nanorod structures was formed in the AAO nanopores.

The XRD patterns of Sn films containing an array of nanotubes deposited at RT (4 min) and 250 °C (3 min) are shown in Fig. 6. The broad peak at about 26 degree can be indexed to SnO, which comes from the natural oxidation on the surface of Sn films since the samples were

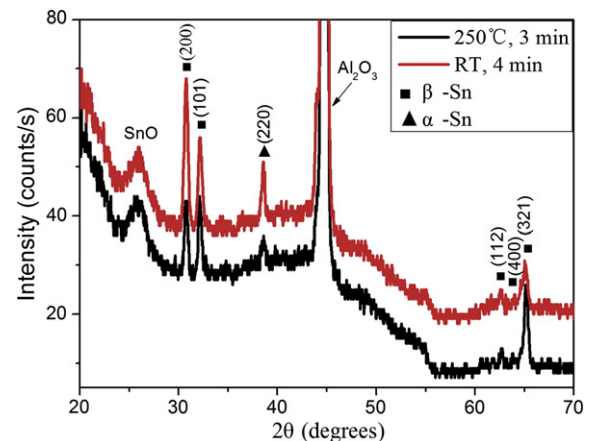


Fig. 6. XRD patterns of isolated Sn nanotube arrays (red line) and cross-linked Sn nanotube arrays (black line).

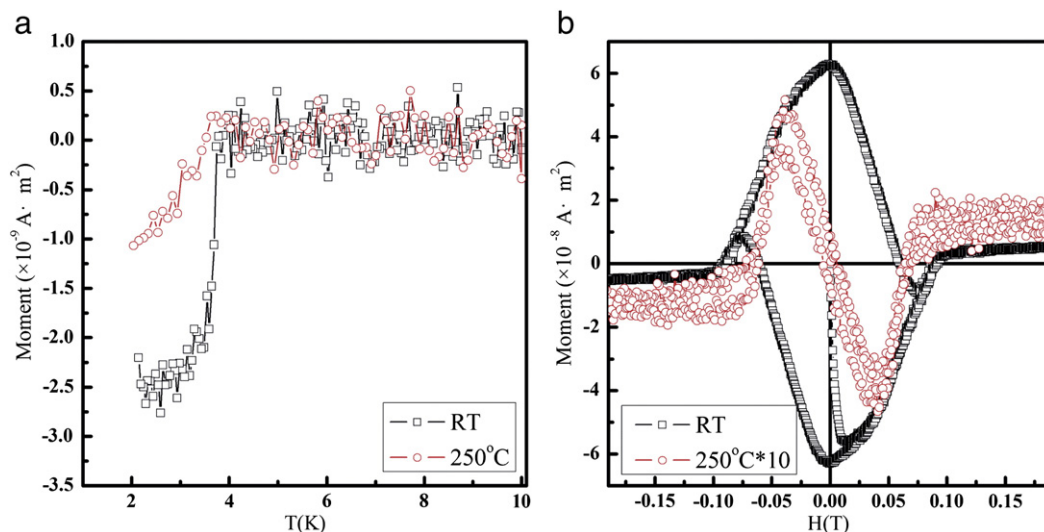


Fig. 7. (a) M–T curves of isolated and cross-linked Sn nanotube arrays measured at 0.01 T magnetic field. (b) M–H curves of the Sn nanotube arrays with different morphologies at 2 K.

stored in atmosphere before the XRD measurement. The results show that the two Sn nanotube arrays both contain polycrystalline structures and there is a coexistence of α -Sn (JCPDS 10-0173) and β -Sn (JCPDS 4-0673) in the Sn films obtained at RT. For the Sn films prepared at 250 °C, the main component was almost completely converted into β -Sn and only a small amount of α -Sn can be observed. The patterns show very much similar (101) peak for both arrays but present a decrease in the intensity of the (200) peak and increase of the (321) peak for the 250 °C-deposited film compared to that of the film deposited at RT. Since the high-index facets possess high surface energy [30], the RT deposition may induce the growth of Sn film with a preferable low surface energy (200) plane. Whereas the 250 °C deposition lead to Sn ion got more energy during the growth and thus high-index facets (321) with higher surface energy was promoted and simultaneously (200) plane with lower surface energy was suppressed. A similar decrease of (200) peak has been observed for gold nanocrystal cubes to octahedral with higher-index facets [31]. So the phase transformation and the changing of the peak intensity can be attributed to a promoted nucleation process and optimized growth orientation at elevated temperature, which lead to a better crystalline property.

The superconducting properties of the nanotube arrays were measured by PPMS with magnetic field perpendicular to nanotube arrays. Fig. 7(a) show the M–T curve for isolated Sn nanotube arrays and crossed-linked Sn nanotube arrays with a field of 0.01 T, respectively. It is observed that both of these two samples show a transition temperature (T_c) value close to the critical temperature of bulk Tin (3.7 K). Fig. 7(a) shows M–H data for isolated Sn nanotube arrays at 2 K. The result is similar to the observation of Tian et al. [14] in single-crystal tin wires. The slight irreversibility behavior in our polycrystalline Sn nanotubes indicates the existence of pinning of magnetic flux which can be attributed to the defects in the nanotubes [32]. Nevertheless, the M–H curve of cross-linked nanotube arrays (Fig. 7(b)) shows a larger magnetic hysteresis which is similar to the typical hard superconductor that has been explained by Bean critical current model [33,34] and Kim-Anderson model [35]. The larger magnetic hysteresis existed in this kind of Sn films can be explained by its worse crystalline quality formed at RT, thus providing more defects for pinning of magnetic flux compared to the Sn films prepared at high temperature. What's more, the isolated nanotube arrays' sample shows a moment one order of magnitude lower than the crossed-linked arrays which is considered associated with the morphologies, that is, the nanotube arrays formed at 250 °C composed of isolated nanocrystals that possess a lower weight/unit area thus lead to the decreasing of the moment in

comparison with the crossed-linked arrays formed at RT which with a film fully covered on AAO template.

4. Conclusions

Vertically Sn nanotube arrays of approximately 500 nm length, 350 nm gap and changing diameter were fabricated using magnetron sputtering and AAO template. Two kinds of morphologies were gained by controlling the substrate temperature during sputtering. The Sn film deposited on AAO film at RT exhibited a wet property and resulted in a cross-linked Sn nanotube arrays. In contrast, with an increased substrate temperature, isolated Sn nanotube arrays were obtained. The different morphologies and crystalline properties affect the superconducting properties of the arrays. The isolated and cross-linked Sn nanotube arrays exhibited superconducting properties which are analogous to single-crystal Sn nanowires and typical hard superconductor, respectively. This research presents a viable approach to fabricate ordered Sn-Pt bimetallic nanotube arrays toward alloy electrocatalysts for methanol oxidation. Furthermore, this technique can be employed as a general method for synthesis of some noble metals such as gold and silver with desirable array patterns and sizes for the application of surface-enhanced Raman scattering (SERS) through the rational control of the experimental conditions.

Acknowledgements

This work was supported by the Natural Science Foundation of China (grant NO. 10874115, 11174197), National Major Basic Research Project of 2012CB934302, National 863 Program 2011AA050518.

References

- [1] Z.Y. Fan, D.W. Wang, P.C. Chang, W.Y. Tseng, J.G. Lu, *Appl. Phys. Lett.* 85 (2004) 5923.
- [2] B.Q. Sun, H. Siringhaus, *J. Am. Chem. Soc.* 128 (2006) 16231.
- [3] Y.B. Li, T. Tokozono, M. Liao, M. Zhong, Y. Koide, I. Yamada, J.-J. Delaunay, *Adv. Funct. Mater.* 20 (2010) 3972.
- [4] X.S. Fang, S.L. Xiong, T.Y. Zhai, Y. Bando, M.Y. Liao, U.K. Gautam, Y. Koide, X.G. Zhang, Y.T. Qian, D. Golberg, *Adv. Mater.* 21 (2009) 5016.
- [5] W.U. Huynh, J.J. Dittmer, A.P. Alivisatos, *Science* 295 (2002) 2425.
- [6] M. Law, L.E. Greene, J.C. Johnson, R. Saykally, P.D. Yang, *Nat. Mater.* 4 (2005) 455.
- [7] K. Shankar, J.I. Basham, N.K. Allam, O.K. Varghese, G.K. Mor, X.J. Feng, M. Paulose, J.A. Seabold, K.S. Choi, C.A. Grimes, *J. Phys. Chem. C* 113 (2009) 6327.
- [8] A. Kongkanand, R.M. Domínguez, P.V. Kamat, *Nano Lett.* 7 (2007) 676.
- [9] Z.L. Wang, *NanoToday* 5 (2010) 540.
- [10] R. Augamuthu, P. Byers, M. Lutz, A.L. Spek, E. Bouwman, *Science* 327 (2011) 313.

- [11] Y.G. Guo, J.S. Hu, H.M. Zhang, H.P. Liang, L.J. Wan, C.L. Bai, *Adv. Mater.* 17 (2005) 746.
- [12] S. Habouti, M. Mátéfi-Tempfli, C.H. Solterbeck, M. Es-Souni, S. Mátéfi-Tempfli, M. Es-Souni, *NanoToday* 6 (2011) 12.
- [13] B. Sepúlveda Martínez, P.C. Angelomé, L.M. Lechuga, L.M. Liz-Marzán, *NanoToday* 4 (2009) 244.
- [14] M.L. Tian, J.G. Wang, J. Snyder, J. Kurtz, Y. Liu, P. Schiffer, T.E. Mallouk, M.H.W. Chan, *Appl. Phys. Lett.* 83 (2003) 1620.
- [15] M.L. Tian, J.G. Wang, J.S. Kurtz, Y. Liu, M.H.W. Chan, T.S. Mayer, T.E. Mallouk, *Phys. Rev. B* 71 (2005) 104521.
- [16] Y.J. Hsu, S.Y. Lu, *J. Phys. Chem. B* 109 (2005) 4398.
- [17] Y.J. Hsu, S.Y. Lu, Y.F. Lin, *Small* 2 (2006) 268.
- [18] M.J. Zheng, G.H. Li, X.Y. Zhang, S.Y. Huang, Y. Lei, L.D. Zhang, *Chem. Mater.* 13 (2001) 3859.
- [19] W. Lee, R. Scholz, K. Nielsch, U. Gösele, *Angew. Chem.* 117 (2005) 6204.
- [20] A.P. Li, F. Müller, A. Birner, K. Nielsch, U. Gösele, *Appl. Phys. Lett.* 84 (1998) 6023.
- [21] H. Masuda, K. Fukuda, *Science* 268 (1995) 1466.
- [22] H. Masuda, K. Yada, A. Osaka, *Jpn. J. Appl. Phys.* 37 (1998) L1340.
- [23] A. Pereira, F. Laplante, M. Chaker, D. Guay, *Adv. Funct. Mater.* 17 (2007) 443.
- [24] Z. Long, J.M. Valles, *J. Low Temp. Phys.* 139 (2005) 429.
- [25] N. Pavenayotin, M.D. Stewart, A.J. Yin, J.M. Xu, *Appl. Phys. Lett.* 87 (2005) 193111.
- [26] K.J. Alvine, O.G. Shpyrko, P.S. Pershan, K. Shin, T.P. Russell, *Phys. Rev. Lett.* 97 (2006) 175503.
- [27] F. Casanova, C.E. Chiang, C.P. Li, I.V. Roshchin, A.M. Ruminski, M.J. Sailor, I.K. Schuller, *Nanotechnology* 19 (2008) 315709.
- [28] F. Casanova, C.E. Chiang, C.P. Li, I.V. Roshchin, A.M. Ruminski, M.J. Sailor, I.K. Schuller, *Europhys. Lett.* 81 (2008) 26003.
- [29] D. Losic, J.G. Shapter, J.G. Mitchell, N.H. Voelcker, *Nanotechnology* 16 (2005) 2275.
- [30] N. Tian, Z.Y. Zhou, S.G. Sun, Y. Ding, Z.L. Wang, *Science* 316 (2007) 732.
- [31] D. Seo, J.C. Park, H. Song, *J. Am. Chem. Soc.* 128 (2006) 14863.
- [32] J.D. Livingston, *Phys. Rev.* 129 (1963) 1943.
- [33] C.P. Bean, *Phys. Rev. Lett.* 8 (1962) 250.
- [34] C.P. Bean, *Rev. Mod. Phys.* 36 (1964) 31.
- [35] Y.B. Kim, C.F. Hempstead, A.R. Strnad, *Phys. Rev.* 129 (1963) 528.